© 2015. Published by The Company of Biologists Ltd | Journal of Cell Science (2015) 128, 3375-3385 doi:10.1242/jcs.166330

RESEARCH ARTICLE

Volume regulation and shape bifurcation in the cell nucleus

Dong-Hwee Kim[1,2,3,*], Bo Li[1,4,*], Fangwei Si[1,4], Jude M. Phillip[1,2], Denis Wirtz[1,2,‡] and Sean X. Sun[1,4,‡]

ABSTRACT

Alterations in nuclear morphology are closely associated with essential cell functions, such as cell motility and polarization, and correlate with a wide range of human diseases, including cancer, muscular dystrophy, dilated cardiomyopathy and progeria. However, the mechanics and forces that shape the nucleus are not well understood. Here, we demonstrate that when an adherent cell is detached from its substratum, the nucleus undergoes a large volumetric reduction accompanied by a morphological transition from an almost smooth to a heavily folded surface. We develop a mathematical model that systematically analyzes the evolution of nuclear shape and volume. The analysis suggests that the pressure difference across the nuclear envelope, which is influenced by changes in cell volume and regulated by microtubules and actin filaments, is a major factor determining nuclear morphology. Our results show that physical and chemical properties of the extracellular microenvironment directly influence nuclear morphology and suggest that there is a direct link between the environment and gene regulation.

KEY WORDS: Cell nucleus, Volume change, Mechanics, Multi-bifurcations

INTRODUCTION

The nucleus is the largest organelle in eukaryotic cells (Gundersen and Worman, 2013; Dahl et al., 2008) and contains most of the cellular genetic material. It is the site of major cellular functions, such as DNA replication, transcriptional regulation, RNA processing and ribosome maturation and assembly. The main mechanical structure that separates the nuclear content from the cytoplasm is the nuclear envelope, which is primarily composed of a double membrane and the underlying nuclear lamina (Simon and Wilson, 2011). The lamina is a network of A- and B-type lamins, and is a stable and viscoelastic material surrounding chromosomal DNA and chromatin (Beaudouin et al., 2002). It is known that the geometrical shape of the nucleus is related to many physiologically important functions of cells and, in particular, to several human diseases (Bissell et al., 1999; Zink et al., 2004; Lammerding et al., 2005; Shimi et al., 2010; Chow et al., 2012). However, the mechanical forces influencing the shape of the nucleus in live cells are not fully understood. Recently, factors affecting nuclear shape have been identified in yeast and *Arabidopsis* (Laporte et al., 2013; Tamura et al., 2013), and external osmotic pressures have been shown to change cell and nuclear volumes of chondrocytes by ±50% in both 2D and 3D cultures (Irianto et al., 2013). Here, we quantitatively examine forces shaping the nucleus using a combination of experiments and physical modeling. We find that, depending on the cellular environment and cell adhesion to the substrate, the nuclear volume can change by 50% in a variety of cells. Highly irregular nuclear shapes can result from mechanical buckling of the nuclear envelope in response to changes in cytoplasmic osmotic pressure. Cytoskeletal motors also directly influence the nuclear shape: microtubule motors apply an overall compressive pressure, whereas actin stress fibers apply compressive forces on the nucleus.

In vivo, the nucleus is typically spherical or ellipsoidal; however, it can undergo dramatic morphological changes in response to physical or environment alterations (Dahl et al., 2008; Aebi et al., 1986; Dauer and Worman, 2009; Hampoelz et al., 2011; Gerlitz et al., 2013; Roca-Cusachs et al., 2008). The nuclear morphology is also correlated with the morphology of the cell – elongated cells typically exhibit an elongated nucleus (Khatau et al., 2009; Versaevel et al., 2012; Weiss and Garber, 1952). These observations suggest that cells can actively control the nuclear morphology. Changes in nuclear shape and volume, in turn, might change nuclear protein concentration, and gene regulation and transcription. Given that adhesion to the extracellular environment affects cell morphology and cellular cytoplasmic organization, and cell morphology affects nuclear morphology, a direct physical link between the environment and gene regulation is possible. To decipher this link, we gradually detached adhered cells from a 2D substrate and into a 3D suspension, and monitored real-time changes in cell and nuclear morphology using 3D confocal microscopy. By depolymerizing perinuclear actin stress fibers and cytoplasmic microtubules, and monitoring corresponding changes in cell and nuclear morphology, we also effectively perturbed forces exerted by actin and myosin motor proteins (Kim et al., 2014; Kim and Wirtz, 2015). To mathematically explain the nuclear shape and volume, we modeled the nuclear envelope as a hyperelastic material obeying a neo-Hookean constitutive relationship. This approach is reasonable because lamin is a stiff intermediate-filament biopolymer. The lamin network in the nuclear envelope in live cells has been shown to be mechanically stable and exhibit slight turnover of lamin A and C in interphase (Swift et al., 2013; Buxboim et al., 2014) and larger changes in division (Beaudouin et al., 2002). Moreover, although mechanical behaviors of lamin networks have been shown to be viscoelastic (Panorchan et al., 2004; Swift et al., 2013), we are interested in the long-term (tens of minutes) behavior of nuclear shape and volume. Therefore, the viscous component of the mechanical response will affect the rate of nuclear shape and volume relaxation but not the final steady shape and volume. The nuclear envelope is also directly permeable to water (Dahl et al., 2004), but the transport of other molecules during interphase is carefully regulated by Ran and its guanine nucleotide exchange factor RCC1 (Macara, 2001; Abu-Arish et al., 2009). The high concentration of genetic material and nuclear chromatin inside the nucleus also suggests that the osmotic pressure across the nuclear

[1]Johns Hopkins Physical Sciences-Oncology Center, Johns Hopkins University, Baltimore, MD 21218, USA. [2]Department of Chemical and Biomolecular Engineering, Johns Hopkins University, Baltimore, MD 21218, USA. [3]Disease Biophysics Group, Wyss Institute for Biologically Inspired Engineering, School of Engineering and Applied Sciences, Harvard University, Cambridge, MA 02138, USA. [4]Department of Mechanical Engineering, Johns Hopkins University, Baltimore, MD 21218, USA.
*These authors contributed equally to this work

[‡]Authors for correspondence (wirtz@jhu.edu; ssun@jhu.edu)

Received 8 December 2014; Accepted 27 July 2015

Journal of Cell Science (2015) 128, 3375-3385 doi:10.1242/jcs.166330

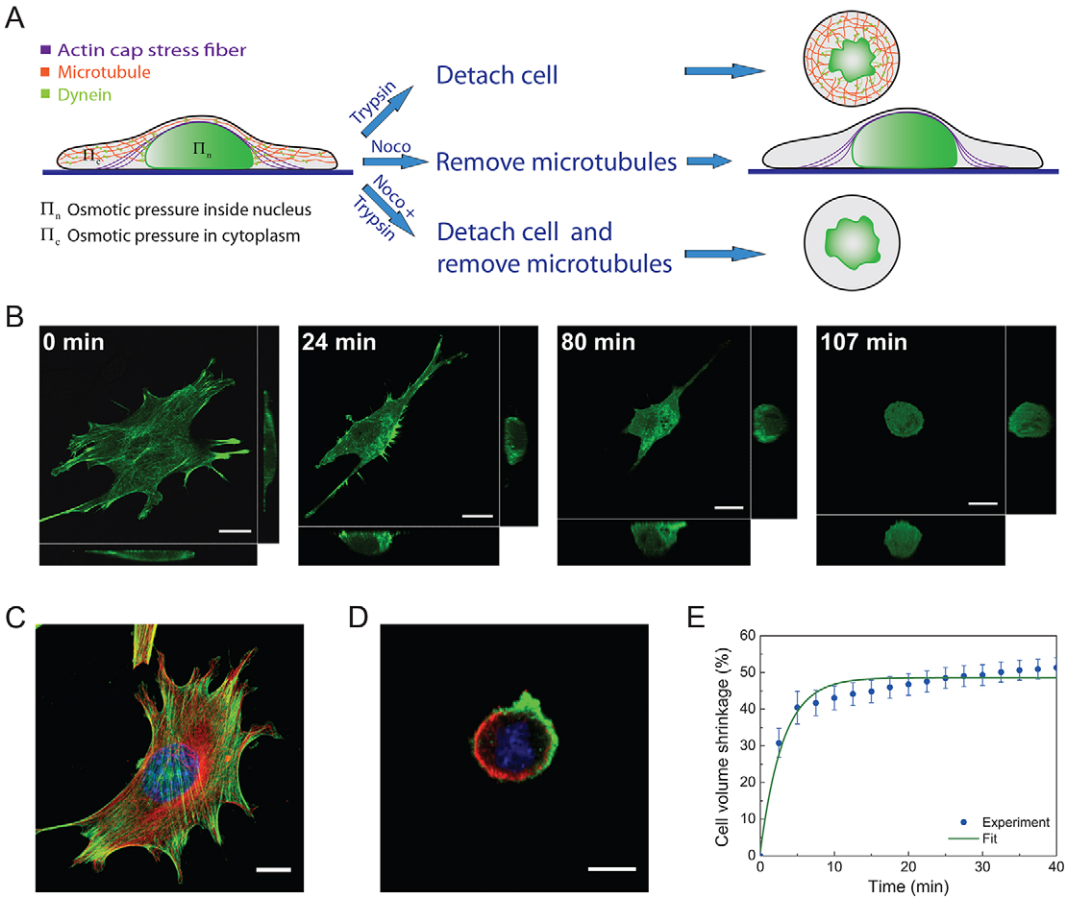

Fig. 1. Cell shape and volume changes upon detachment from the substrate. (A) In the adherent state, both actin filaments and microtubules apply forces on the nucleus. Upon cell detachment, actin stress fibers no longer surround the nucleus and become cortical. Addition of nocodazole removes microtubules. We independently perturb actin and microtubules using a combination of cell detachment and nocodazole (Noco) as illustrated in the schematic. (B) Confocal fluorescent images of a MEF transfected with GFP–lifeact. Upon mild trypsin treatment, the cell gradually detached from the substrate and its shape became more round. (C) Actin filaments (green) and microtubules (red) in an adhered cell. Microtubules surround the DAPI-stained nucleus (blue). This image is also shown as a control in Fig. 5A. (D) Actin filaments (green) and microtubules (red) in the suspended cell. Actin is cortical and microtubules surround the nucleus (blue). (E) Percentage reduction in MEF cell volume during the detachment from the substrate. The green line is fitted to the measured volume reduction over time (blue circles). The data are mean±s.e.m. obtained from 35 independent live cells (>10 cells per trial, repeated three times). Scale bars: 10 µm.

envelope is unequal. We show that with this combination of assumptions together with quantitative measurements, we are able to estimate the nuclear osmotic pressure difference and cytoskeletal mechanical forces experienced by the nucleus. If changing environmental factors affects cytoskeletal forces and cell morphology, our model is able to predict how nuclear morphology responds to environmental changes.

RESULTS

We first examined time-dependent changes in nuclear volume and shape while an adherent mouse embryonic fibroblast (MEF) was gradually detached from the substrate (Fig. 1). The cell evolved from a flat and spread shape to a rounded one and, finally, became essentially a sphere when it was suspended (Fig. 1B). Our real-time single-cell monitoring showed that the cell volume in the detached state reduced to approximately one half of its initial attached volume (Fig. 1E). Concurrently, the nuclear volume also decreased: after about 10–20 min, the nuclear volume had reduced by 50% (Fig. 2). During nuclear volume shrinkage, the nuclear envelope developed multiple wrinkles and became highly irregular in shape (Fig. 2A). The same dramatic decrease in nuclear volume was also observed in other types of cells [e.g. human foreskin fibroblast (HFF) cells; see Fig. 3].

Volume change in the nucleus

We next considered possible active cellular forces driving these changes in nuclear shape and volume. In an adherent cell, a perinuclear actin cap, made of an array of contractile stress fibers, is present on the top and sides of the interphase nucleus (Kim et al., 2013). Upon cell detachment, both basal and actin cap stress fibers disappeared and actin filaments became entirely cortical (Fig. 1C,D). During actin filament remodeling, the nucleus evolved from a flat pancake shape to a more rounded shape. Eventually, as the cell fully detached, the nuclear volume shrank as indicated in Fig. 2C. Depolymerizing actin filaments in the attached cell using low levels of latrunculin initially resulted in a slight increase in nuclear volume (Fig. 2F), and subsequently resulted in similar volume and shape changes to those observed when detaching the cell. Treating the cell with ML7, which prevents myosin phosphorylation, also resulted in a slight increase in nuclear volume (Fig. 2E). These results suggest that, in the attached state, actin stress fibers apply a compressive force on the nucleus. Next, we monitored cells treated with nocodazole, which depolymerizes microtubules. In the adherent cell, the nuclear volume became larger upon nocodazole treatment (Table 1). If the cell detached, the nuclear volume also decreased, but to a lesser extent than control cells (~40%) (Fig. 2D); however, the irregular nuclear shape

Journal of Cell Science (2015) 128, 3375-3385 doi:10.1242/jcs.166330

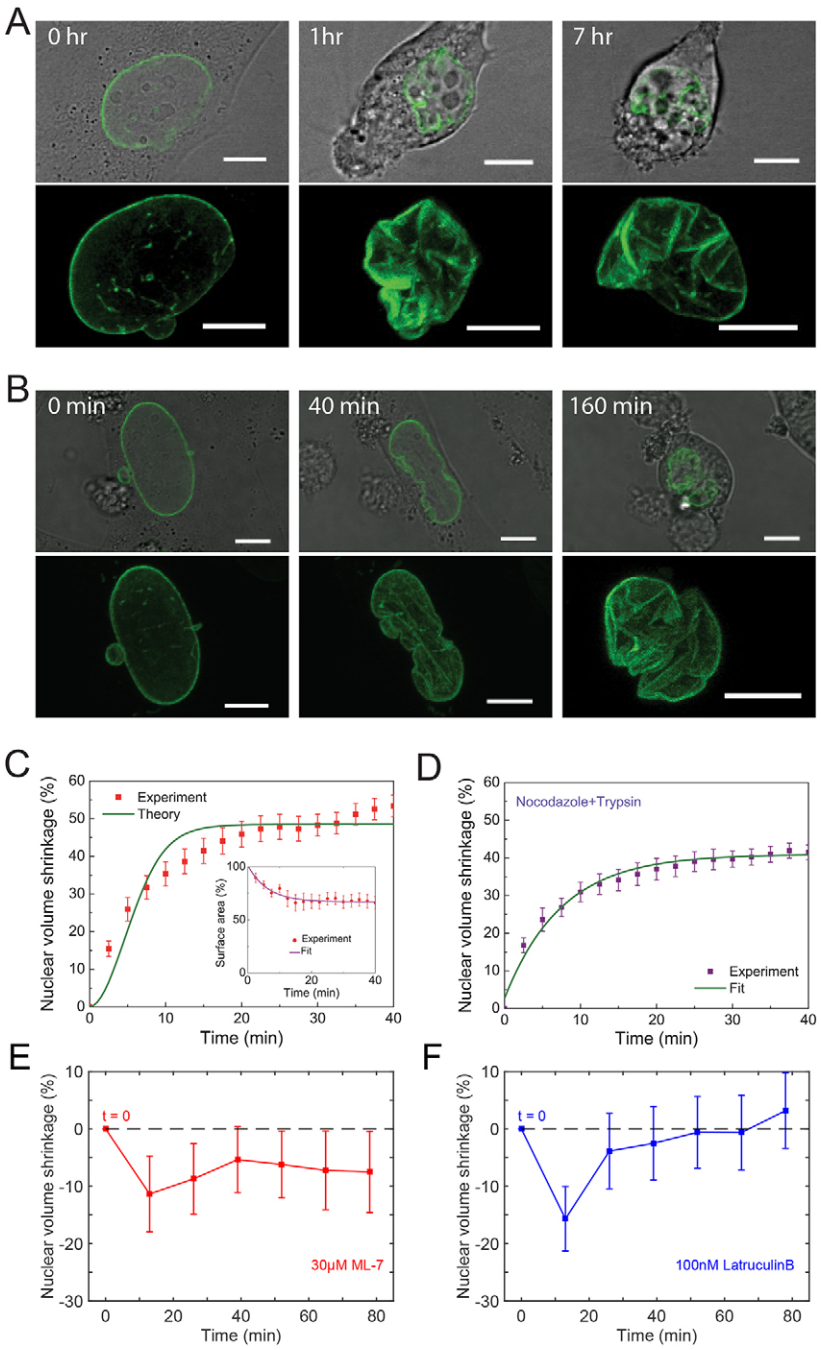

Fig. 2. Wrinkling and volume shrinkage of the nucleus. (A) A GFP–lamin-A-transfected MEF treated with trypsin showing the progressively wrinkling nucleus as the cell detaches from the collagen-coated glass-bottomed dish. The upper panels are DIC and GFP channel merged images and the lower panels are enlarged GFP channel images showing details of nuclear morphology. (B) Trypsinization of a GFP–lamin-A-transfected MEF pre-treated with nocodazole. The nucleus undergoes a similar shape change to the control. (C) Experimental measurement and theoretical prediction of nuclear volume shrinkage during cell detachment. The theoretical curve is explained in the Materials and Methods. The data are mean±s.e.m. obtained from 37 live cells (>10 cells per trial, repeated three times). Inset: the change in the surface area of the nucleus during detachment. (D) The shrinkage in nuclear volume of nocodazole pre-treated MEF cells during cell detachment. The volume shrinks to a lesser extent than in control cells. Results are mean±s.e.m. for 31 cells (5–10 cells per trial, repeated four times) were tested and results are (E) Nuclear volume shrinkage in attached MEF cells treated with ML-7 (mean±s.e.m., 10 cells were tested). Upon treatment the nuclear volume slightly increased, suggesting that myosin exerts a compressive force on the nucleus. (F) Nuclear volume shrinkage in attached MEF cells treated with low levels of LatB (mean±s.e.m., 10 cells were tested). The nuclear volume initially increased slightly, and then as the cell detached, began to decrease. Taken together with data in E, this suggests that actomyosin stress fibers are compressing the nucleus in the attached state. Scale bars: 10 μm.

remained similar to that in control cells. Consistent with previous studies (Hampoelz et al., 2011; Gerlitz et al., 2013; Zhao et al., 2012), these volumetric measurements suggest that, through microtubule motors, the microtubule network also exerts compressive forces on the nucleus.

At the scale of hundreds of cubic micrometers, changes in nuclear volume must coincide with material (mostly water) entering and existing the nucleus. Indeed, the nuclear pore complex in the nuclear envelope is directly permeable to water (Dahl et al., 2004). The flux of water, in turn, is controlled by both osmotic and hydrostatic pressure differences across the envelope. Mechanical forces on the nuclear envelope indirectly impact on the hydrostatic pressure difference between the cytoplasm and the nucleus. Although small proteins and RNA can enter and exit the nucleus, the net solute flux is likely quite small when compared with high concentration of nuclear DNA and chromatin. Therefore, in this treatment, we assume that the nuclear–cytoplasmic transport of solutes is negligible. We can mathematically estimate the nuclear volume V_n during cell detachment using an equation for the flux of water (Salbreux et al., 2007; Jiang and Sun, 2013):

$$\frac{dV_n}{dt} = \alpha(\Delta\Pi_n - \Delta P_h), \quad (1)$$

where α is the hydraulic permeability of the nuclear envelope and $\Delta\Pi_n$ is the difference in the osmotic pressure in the nucleus and the cytoplasm ($\Pi_n - \Pi_c$). The osmotic pressure in the cytoplasm depends on the cell volume: $\Pi_c = N_c RT/V_c$, where N_c is the total solute in the cytoplasm. V_c is the cytoplasmic volume, which decreases as the cell detaches. The osmotic pressure Π_n inside the nucleus can be calculated similarly. ΔP_h denotes the hydrostatic

Journal of Cell Science (2015) 128, 3375-3385 doi:10.1242/jcs.166330

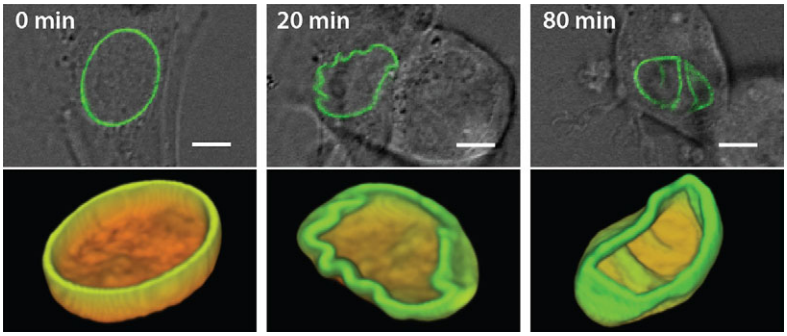

Fig. 3. Wrinkling of the nucleus envelope in a HFF cell treated with trypsin. The nuclear volume shrank by 38%. Scale bars: 5 µm.

pressure difference, which is balanced by pressures applied by the cytoskeleton and the mechanical resistance of the nuclear envelope. During cell detachment, we measured the cytoplasmic volume reduction as a function of time, therefore changes in $\Delta\Pi_n$ in Eqn 1 are known. We also can independently remove the influence of actin stress fibers and microtubules, and measure the nuclear volume before and after cell detachment (Fig. 1A). These experiments allowed us to estimate the cytoskeletal forces on the nucleus. Detailed mathematical analysis is given in the Materials and Methods.

When the cell is attached to the substrate (Fig. 4A), the shape of the nucleus resembles a pancake (Fig. 4B). In this state, we conjecture that the osmotic pressure inside the nucleus is larger than that of the cytoplasm, and the nucleus is inflated; otherwise, the envelope would buckle and invaginate laterally, as demonstrated by our theoretical model (Fig. 4B,C). From our nuclear shape and volume measurements on cells treated with nocodazole (Table 1; Fig. 5) where only actin stress fibers remain, we find that the actin-based force is $F/(\pi r_a^2\mu)\approx 8.16\times10^{-2}$ in the attached state, where μ denotes the effective shear modulus of the nuclear envelope and r_a is the radius of the actin contact region on top of the nucleus. μ cannot be obtained from the model directly. Instead, we can obtain ratios, such as $F/(\pi r_a^2\mu)$. If we assume that the nuclear envelope behaves as a typical biofilament network, then μ is on the order of 10^2–10^4 Pa, which implies that the compressive actin force exercised by the perinuclear actin cap is on the order $F\approx$1–100 nN. This result is consistent with traction force microscopy measurements of cell contractile forces (Munevar et al., 2001; Sabass et al., 2008). Next, from the change in nuclear volume before and after the addition of nocodazole, we deduce that microtubules apply a compressive pressure on the order of 10–100 Pa (see Materials and Methods).

From these estimated cytoskeletal forces, we can predict the nuclear volume in detached cells without microtubules. Our prediction is in good agreement with measurements, as shown in Fig. 2C. During cell detachment, because the cytoplasmic osmotic pressure decreases dramatically, water flows out of the nucleus and the nuclear volume shrinks.

To verify that the observed nuclear shape transformations are reversible, we performed experiments that re-attached a suspended cell (Fig. 6A). Our results show that the shapes are fully reversible and consistent with our mechanical pictures of the nucleus. Quantitative results on nuclear volume in this reverse experiment are shown in Fig. 6B. Moreover, it is not necessary to detach cells to observe nuclear volume changes. We also applied hypertonic shock to attached cells by adding cell culture medium supplemented with 50% (v/v) polyethylene glycol and observed correlated changes in cell and nuclear volume (Fig. 6C). The volume measurement was performed at 10 min after shock. In this case, the result is consistent with the idea that there is an osmotic pressure difference and no substantial protein transport across the nuclear envelope. If there is protein transport, the osmotic pressure difference should equilibrate and the nuclear volume would remain the same.

In addition, we observed that the nuclear volume was reduced when cells were placed on extremely soft polyacrylamide hydrogels (Young's modulus ~1 kPa), corresponding to the elasticity of brain tissues (Georges et al., 2006; Buxboim et al., 2010; Swift et al., 2013), and that the nuclear surface was also wrinkled (see figure 3D in Swift et al., 2013 and figure 3K in Kim and Wirtz, 2015). See supplementary material Fig. S3 for details.

Table 1. Measured nucleus data for adhered MEFs

Description	Before adding nocodazole	After adding nocodazole
Volume (µm^3)	880.89 (±78.00)	930.09 (±80.12)
Surface area (µm^2)	712.91 (±34.16)	751.93 (±34.35)
Radius of the contacting region (µm)	7.69 (±0.23)	7.87 (±0.22)

36 cells were used to obtain mean±s.e.m. values.

Shape bifurcation in the nucleus

The above analysis provides a physical mechanism for the large volume shrinkage of the nucleus during the detachment process. The question remains as to the origin of the wrinkled nucleus after full detachment (Fig. 2A,B). Previous experiments have shown that the eukaryotic lamin network behaves as an elastic solid and the elastic properties of nucleus originate largely from the lamin network rather than the interior contents (Beaudouin et al., 2002; Dahl et al., 2004). The lamina is also several tens of nanometers in thickness (Dahl et al., 2004; Funkhouser et al., 2013; Vaziri et al., 2006; Wirtz et al., 2011). Therefore, to describe the equilibrium steady-state shape of the nucleus, it is sufficient to treat it as an elastic shell. However, the observed mechanical deformations are large, and linear elasticity is not adequate. To incorporate nonlinear large deformation effects, we use a neo-Hookean model (Ogden, 1997) to describe nuclear mechanics. Note that the time-dependent mechanical responses of nucleus will show viscoelastic characters from a combination of factors (Funkhouser et al., 2013; Vaziri et al., 2006; Guilak et al., 2000). However, viscous effects should only influence the dynamics of relaxation to the steady-state shape but not the final shape itself. In our cell detachment experiments, the cell volume decreased dramatically (Fig. 1), which raises the cytoplasmic osmotic pressure, such that the net pressure across the nuclear envelope changes from positive to negative. (Here, we define the pressure along the outward radial direction to be positive.) We can analyze the shape and volume of the nucleus as a function of the changing pressure. The non-linear mechanical model predicts that the

Journal of Cell Science (2015) 128, 3375-3385 doi:10.1242/jcs.166330

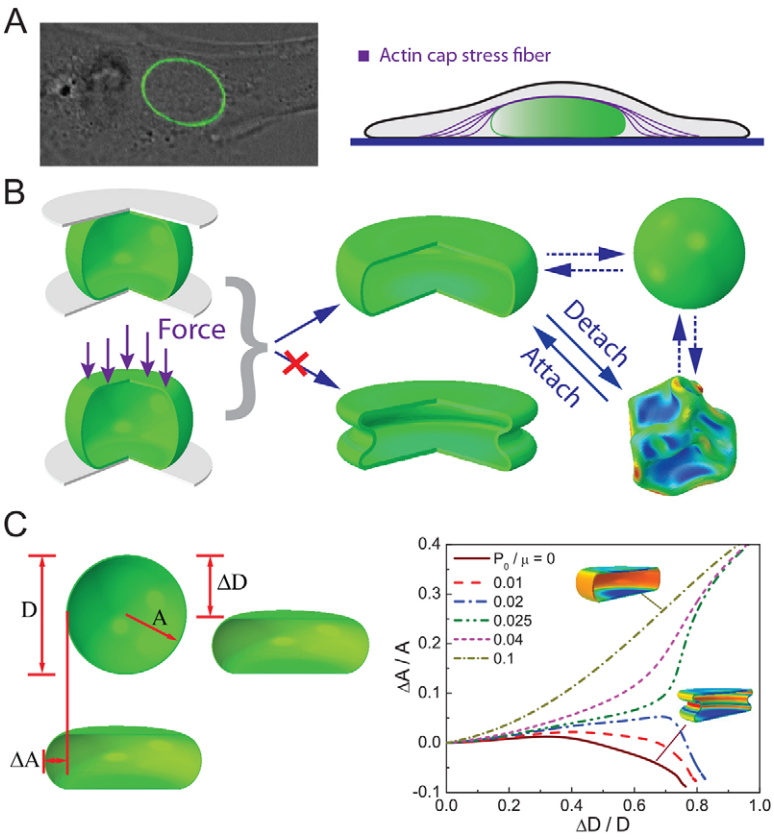

Fig. 4. Nuclei in adherent cells. (A) The nucleus in a GFP–lamin-A-transfected MEF attached to a collagen-coated glass-bottomed dish. The nucleus is compressed by perinuclear actin stress fibers from above. (B) In our model, forces from the perinuclear actin fibers are modeled as a compressive plate. The surrounding microtubules are modeled by a positive mechanical pressure on the nucleus. Our FEM simulations show that in order to obtain the nuclear shape observed in attached cells, the nucleus has to be 'inflated' by a negative pressure; otherwise, the nuclear envelope will buckle and invaginate. As the cell detaches, owing to a large cell volume reduction, the osmotic pressure outside the nucleus becomes larger and the pressure difference becomes positive. The nucleus responds to the changing pressure by developing surface wrinkles. (C) Left, in the adhered state, the nucleus is compressed by actin stress fibers and resembles a pancake. In the deformed state the change in nuclear radius and height are denoted as ΔA and ΔD, respectively. Right, the computed shape of the nucleus in the adherent state. The pressure difference, P_0/μ, must be sufficiently large such that the nuclear envelope will not buckle under actin force, where μ is the shear modulus of the nuclear envelope.

nuclear volume as a function of the pressure difference for a spherical pressurized nucleus (Fig. 7A) is:

$$-P = 2\mu\left(\frac{1-\bar{V}^2}{\bar{V}^{7/3}}\right)\frac{H}{A}, \qquad (2)$$

where $-P$ is the total pressure difference across the nuclear envelope. In the limit of static nuclear volume, this is equal to the pressure applied by microtubules minus the osmotic pressure difference. H and A are the reference thickness and the reference inner radius of nucleus envelope in the stress-free state, respectively, and $\bar{V}=V_n/V_{n0}$, with V_{n0} being the volumes of nucleus at the stress-free state. Note, that this result is only valid when the nucleus maintains spherical geometry. We see that when $-P>0$, $\bar{V}<1$, which implies, as expected, that the nucleus shrinks due to outside compressive pressure. Our experiments show that after cell detachment, the nuclear volume is dramatically reduced (Fig. 2C). If the original spherical symmetry is maintained, this volume reduction requires a very large compressive pressure of $-P/\mu\approx0.1$ for H/A=0.01 and $-P/\mu\approx1$ for H/A=0.03. This implies a compressive pressure of hundreds of kPa. An elastic shell is unable to endure such large pressure differences without shape bifurcation (Hutchinson, 1967). Therefore, a likely explanation of the nuclear wrinkling (Fig. 2A,B) is that the nuclear envelope mechanically buckles under pressure. These bifurcations (buckling) break the spherical symmetry and reduce the nuclear volume. To capture this intriguing morphological transition, we adopt the incremental deformation theory (Ogden, 1997) to analyze the buckling behavior of the nucleus. The wrinkled patterns can be described by a spherical harmonic function with degree n (Lidmar et al., 2003; Ben Amar and Goriely, 2005).

For a given thickness-to-radius ratio, H/A, as the compressive pressure reaches a threshold value, the nucleus bifurcates with a morphology manifested by a mode number, referred as the critical mode, n_{crit}. Fig. 7B illustrates the critical properties of the nucleus. With increasing thickness, the critical mode n_{crit} decreases while the critical volume change, $\Delta V_{crit}/V_{n0}$, increases, where $\Delta V_{crit}=V_{n0}-V_{crit}$, with V_{crit} being the nuclear volume in the critical state. $\Delta V_{crit}/V_{n0}$ scales as $(H/A)^{0.97}$ for a thin envelope (e.g. H/A<0.2), and $\Delta V_{crit}/V_{n0}\approx(H/A)^{0.47}$ for a thick envelope (e.g. H/A>0.5). Given that the thickness-to-radius ratio for nuclei is small ($\sim10^{-3}$–10^{-2}) (Funkhouser et al., 2013), the critical mode scales as $n_{crit}\approx(H/A)^{-0.50}$. In addition, the critical pressure difference scales as $-P_{crit}/\mu\approx(H/A)^2$, which is reminiscent of the prediction for linear elasticity spherical shells (Hutchinson, 1967; Datta et al., 2012), although in our model we consider finite deformations (Fig. 7C). These results suggest that the nuclear wrinkling onset is controlled by geometry (i.e. H/A). For a thinner nuclear envelope, the mode number is larger. However, the critical volume reduction for wrinkling onset is smaller. For the nuclear envelope, with a thickness-to-radius ratio of 0.02, wrinkling and shape bifurcation will take place when the volume reduction reaches just 2%.

Fig. 2C shows that the nuclear volume decreases up to 50%, which is much larger than the critical value of the bifurcation onset discussed above. This indicates that the nucleus is progressively entering into a state far from the first bifurcation (Fig. 7D). Furthermore, our experiments suggest that the nucleus evolves towards a 3D folded pattern, rather than the regular dimple or polygon patterns. To confirm this, we implemented 3D finite element method (FEM) simulations to track the path of pattern evolution. The results demonstrate that two successive bifurcations reduce nuclear volume (Fig. 7E). Fig. 7F,G show the comparison

Journal of Cell Science (2015) 128, 3375-3385 doi:10.1242/jcs.166330

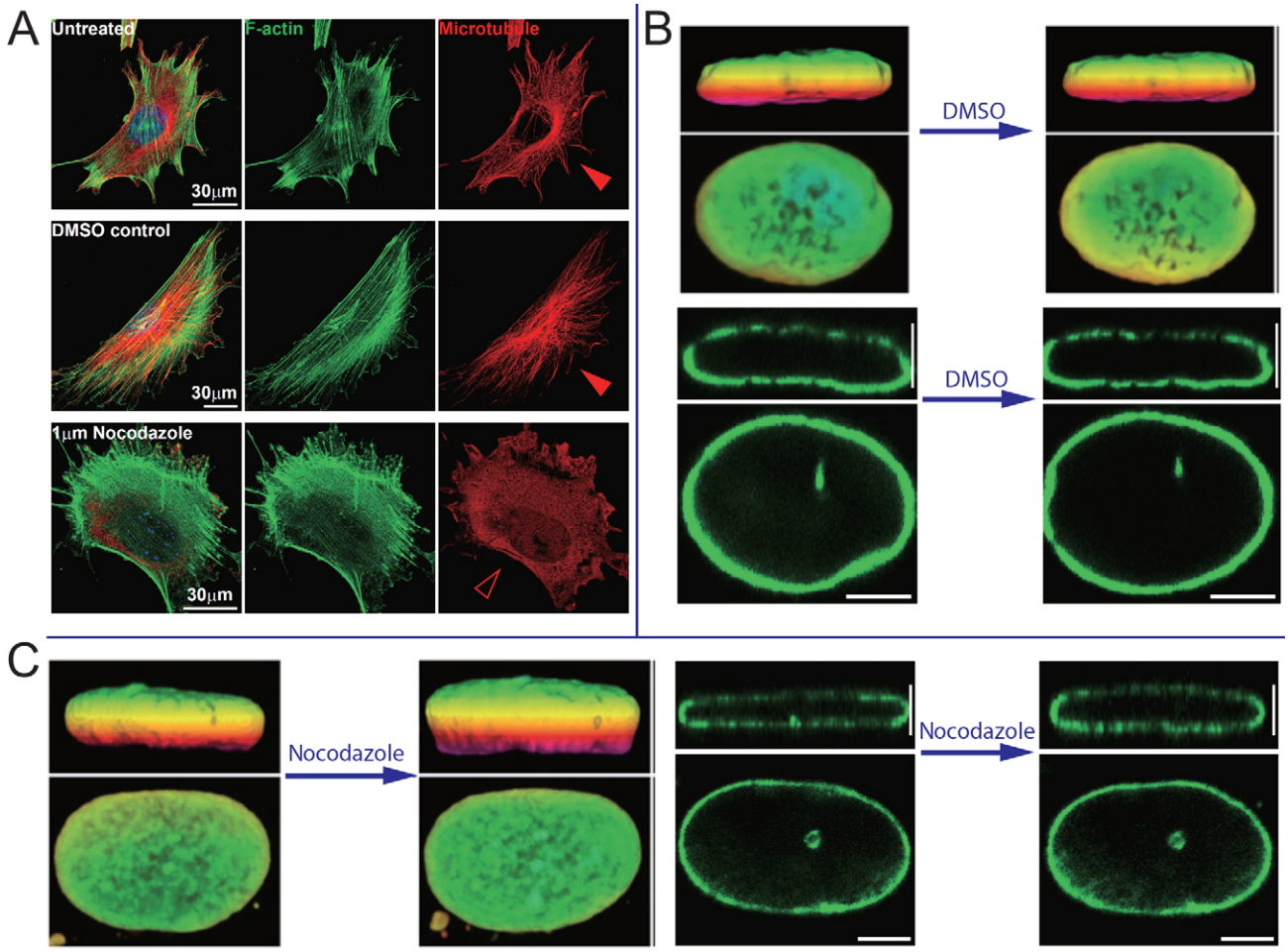

Fig. 5. Cell and nuclear morphology under DMSO and nocodazole treatment. (A) Immunofluorescence images of untreated (this is same example as shown in Fig. 1A), DMSO control and nocodazole-treated MEF cells. Solid and open arrowheads indicate organized and disrupted microtubule networks, respectively. Note that the organization of actin filaments (green) remained intact whereas the α-tubulin-stained microtubule structure (red) was largely disrupted after a given nocodazole treatment (1 μM, 30 min). (B) Images of the nucleus in a DMSO-treated control MEF cell. Upper panel, *z*-depth rendering of the nucleus; lower panel, *xz* and *xy* cross-sectional views. (C) Images of the nucleus in a nocodazole-treated (1 μM, 30 min) MEF cell. Left panel, *z*-depth rendering of the nucleus; right panel, *xz* and *xy* cross-sectional views. Scale bars: 5 μm.

between simulations and experiments: our model is able to accurately reproduce the observed nuclear morphology. Progressive simulations for different geometries were performed (Fig. 7H–J). The volume reduction ratio around the first bifurcation is less than 20%, which is still lower than our experimental measurements. However, an increasing compressive pressure triggers the second bifurcation (the second column in Fig. 7H–J). The dimple patterns formed in the first bifurcation break into folded structures: some dimples narrow into troughs, whereas others merge with their neighbors. In this way, nuclei evolve towards a heavily folded shape and the volume is further reduced. Our simulations demonstrate that volume reduction is able to reach 80%, a level at which self-contact takes place (path 2 in Fig. 7E). Moreover, the second bifurcation and the subsequent evolution lower the mode number but enhance the wavelength due to merging of dimples. This also explains why, although thickness-to-radius ratio is small, the observed number of folds on the surface is not dense and is less than the n_{crit} predicted by the first bifurcation (Quemeneur et al., 2012). From these simulations, we conclude that nuclear shape is strongly regulated by pressure differences across the nuclear envelope, mechanical forces from the cytoplasm, and nuclear envelope geometry.

DISCUSSION

We used a combination of experiments, theory and numerical simulations to decipher the mechanisms controlling the morphology and volume of eukaryotic nuclei. We discover that the adherent nucleus is best described as an elastic envelope inflated by osmotic pressure, and cytoskeletal forces further shape the nucleus, depending on the cell microenvironment. The model is able to reasonably explain nuclear shapes and volumes under a wide range of experimental perturbations, although precise quantitative agreements between model and experiments in Fig. 2 are difficult because the lack of information on remodeling dynamics of the actin stress fibers and microtubule network during cell detachment. When the adherent cell is detached from its substratum, the nuclear volume shrinks to one half of its original size. The observed morphological transition is well captured by an elastic instability and the post-instability evolution far beyond the first bifurcation. We note that the cell and volume measurements in this paper were performed using confocal microscopy (Maeshima et al., 2010). Although accurate measurements of spherical shapes by confocal microscopy can be demonstrated (see the Materials and Methods), it remains to be shown whether accurate volume measurements can be achieved for irregular nuclear shapes (e.g. Fig. 2A,B).

Journal of Cell Science (2015) 128, 3375-3385 doi:10.1242/jcs.166330

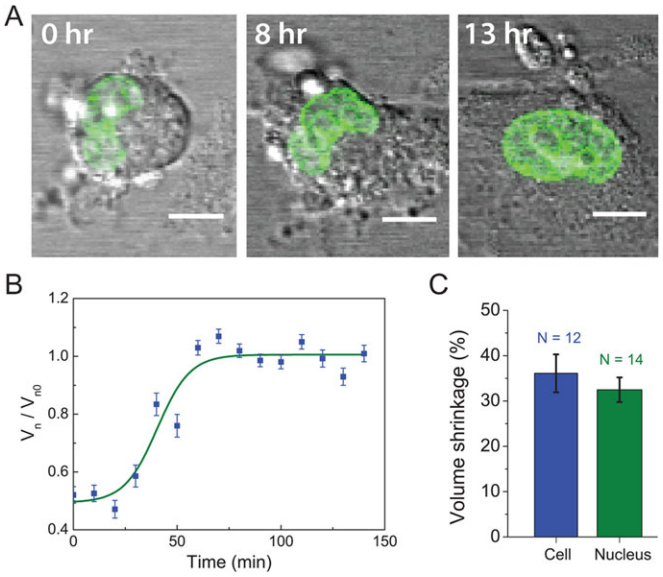

Fig. 6. Nuclear volume change is reversible and consistent with the osmotic shock results. (A) The nuclear shape change is reversible. A GFP–H2B-histone-transfected MEF was initially treated with trypsin. After the cell had detached partially, it was gently washed with pure medium and cell became fully attached. In this process, the nucleus transformed from a wrinkled morphology to a round shape, reversing the shape changes seen in Fig. 2. Scale bars: 10 µm. (B) Volume change in the nucleus of a MEF cell during cell going from the detached state to the attached state (reverse of Fig. 2, see images in A). V_{n0} is the nuclear volume in the adherent state. V_n denotes the nuclear volume during detachment. Results are mean±s.e.m., n=31 cells (>10 cells per trial, as indicated in the figure, repeated three times). (C) Volume reduction after hypertonic shock on adherent cells. A similar volume shrinkage occurred in the cell and the nucleus. Therefore, extracellular osmotic content changes cytoplasmic osmotic pressure, which drives nuclear volume shrinkage.

During the experiments, both MEF and HFF cells were monitored, and similar volume variation and shape bifurcations were observed. Although further experiments on other types of cells are needed, our results demonstrate that there might be general mechanisms regulating nuclear volume and shape in eukaryotic cells. An overlooked aspect of nuclear mechanics is the osmotic pressure difference across the nuclear envelope. Our reversible measurements on MEF cells (Fig. 6) shows that osmotic pressure might be a main driver of nuclear shape change. We note that the nuclear envelope consists of A- and B-type lamins, which might have different mechanical properties and distribute non-uniformly on the nuclear envelope (Funkhouser et al., 2013). Therefore, the nuclear envelope is not isotropic. However, most results presented here would not be qualitatively different if an anisotropic or a heterogeneous nucleus were considered. Furthermore, the nuclear shape changes seen here are only consistent with the behavior of an elastic shell under pressure, and not consistent with a solid deformable object. This suggests that the material inside the nucleus is dynamic and fluid like, and might contain other interesting and unexplored dynamics.

We have shown how the shape and size of the cell can influence nuclear shape and volume, and presumably indirectly influence chemical concentrations of nuclear molecules. Given that the environmental variables such as extracellular matrix properties and external osmotic pressure influence cell size and shape, a direct link might exist between environmental variables and gene regulation through the mechanism proposed here. Indeed, we observed that the nuclear volume was reduced when cells were placed on the extremely soft polyacrylamide hydrogels, and the nuclear surface became wrinkled (supplementary material Fig. S3). For diseases such as cancer, muscular dystrophy, cardiomyopathy, and progeria, our model provides a starting point for a molecular explanation of abnormal nuclear shape, which could lead to the discovery of new disease mechanisms.

MATERIALS AND METHODS

Cell culture

To monitor detachment of live adherent cells, mouse embryonic fibroblasts (MEFs) and human foreskin fibroblasts (HFFs) were cultured in Dulbecco's modified Eagle's medium (ATCC, Manassas, VA) supplemented with 10% fetal bovine serum (ATCC), 100 units/ml penicillin and 100 µg/ml streptomycin (Sigma, St Louis, MO). Cells were maintained at 37°C with 5% CO_2 in a humidified incubator and passaged every 3–4 days. For hypertonic shock on cells, the cell culture medium was supplemented with 50% (v/v) polyethylene glycol (Sigma).

Transient transfection and drug treatment

GFP–lamin-A or GFP–histone-H2B was transfected to monitor nuclear morphology and volume, and GFP–lifeact was transfected to allow the approximate measurement of cell volume. The transient transfection complex was prepared in Opti-MEM I reduced serum medium (Gibco, Carlsbad, CA), and FuGENE HD (Roche, Indianapolis, IN) was used as a transfection agent. DNA loading and composition were determined according to the manufacturer's instructions. The microtubule-depolymerizing drug nocodazole (Sigma) was diluted to a final concentration of 1 µM by using the stock solution. Cells were treated with either DMSO control or nocodazole-containing cell culture medium and incubated for 30 min before imaging.

Cell detachment setup

After allowing cells to spread on a glass-bottomed dish coated with 0.2 mg/ml type-I collagen (BD Biosciences), a dish containing attached cells was transferred to the live-cell chamber (OKO labs) and mounted on a confocal laser microscope (A1, Nikon). To detach cells from the glass-bottomed dishes, cell culture medium was carefully replaced with pre-warmed 0.25% trypsin-EDTA solution (Sigma) without making physical disturbances on the cells being imaged. To monitor cell attachment from the detached state, the trypsin-treated cell was gently washed with pure medium and monitored over time.

Live-cell confocal microscopy and immunofluorescence

Confocal imaging of GFP–lifeact-transfected cells was conducted using a 60× Plan Fluor lens (NA 1.4). Each frame was taken every 4 to 20 min to avoid significant photobleaching during imaging time of up to 6 h. A z-stack of time-lapsed confocal images were processed and analyzed for 3D rendering and volume measurement using NIS elements software (Nikon). 3D reconstructed cell shapes are shown in supplementary material Fig. S4. To visualize the organization of cytoskeleton in the adherent or suspended cells, cells were fixed with 4% paraformaldehyde and permeabilized with Triton X-100 (Fisher biotech). Anti-α-tubulin primary antibody (abcam) and Alexa-Fluor-568-conjugated goat anti-mouse-IgG secondary antibody (Invitrogen) were used to stain microtubules, and actin filaments and nuclear DNA were marked by Alexa-Fluor-488–phalloidin (Invitrogen) and DAPI, respectively.

Nuclear volume and surface area calculation

z-stacks of confocal fluorescent images were also analyzed to calculate the nuclear volume and surface area by using customerized MATLAB (Mathworks, Inc., Natick, MA) scripts (available on request). The 2D GFP–lamin-A or GFP–histone-H2B image in each z-stack was used to localize the outer edge of nuclear envelope by calculating the gradient of intensity across all pixels. The nuclear edge was comprised of pixels whose intensity gradient was higher than a threshold (Sobel gradient operator). This threshold was selected within a range of values where the calculated nuclear volume was independent of the threshold value (the volume was calculated

Journal of Cell Science (2015) 128, 3375-3385 doi:10.1242/jcs.166330

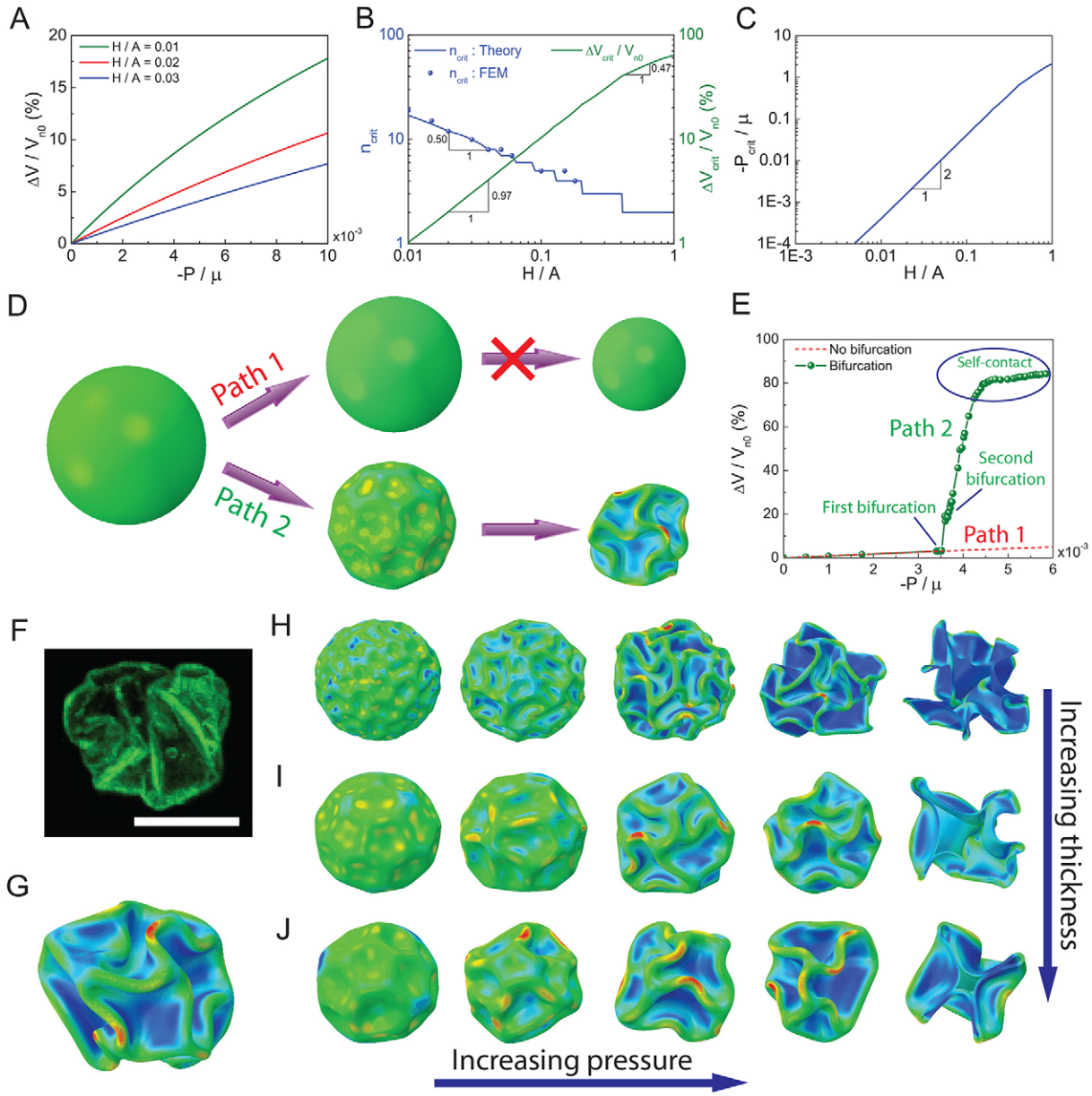

Fig. 7. Model calculations of nuclear deformation and wrinkling. We model the nuclear envelope as an elastic shell with shear modulus μ. (A) Volumetric reduction under compressive pressure from homogeneous deformation for nuclei with different thickness-to-radius ratios (*H*/*A*; Eqn 2). The volume decreases with increasing compressive pressure. (B) With increasing pressure, the nuclear envelope buckles at a critical mode number, n_{crit}. This critical mode number and volume reduction depend on *H*/*A*. The theoretical results are compared to the numerical simulations using the FEM. (C) Dependence of the critical pressure at the onset of buckling on *H*/*A*. (D) Shape of the nucleus with increasing compressive pressure. Path 1 shows homogeneous deformation where the nucleus maintains spherical geometry. Path 2 contains two successive buckling transitions. The first buckling (bifurcation) transition develops regular dimples or polygons paving the nuclear surface. These regular buckling patterns are distorted by the second buckling transition, generating a folded structure. (E) Nuclear volume shrinkage with increasing compressive pressure. Path 1 and 2 are obtained from theoretical analysis and FEM simulation, respectively. (F) Confocal image of a fully buckled nucleus in an MEF cell after complete detachment. Scale bar: 10 μm. (G) Folded nucleus produced by FEM simulation. The thickness-to-radius ratio here is $H/A \approx 0.027$, which appears to match the experimental image. (H–J) FEM simulations of nuclei shape as a function of increasing compressive pressure with thickness-to-radius ratios (*H*/*A*) of 0.01, 0.027 and 0.05, respectively. The last column is a cross-section of a folded nucleus.

as below). Once the outer edge of the nuclear envelope in each stack was determined, a 3D domain of pixels within the edge was integrated to obtain the total nuclear volume. To calculate the nuclear surface area, 3D domain of pixels within the nuclear envelope were enclosed by stitching the smallest triangular patches that cover the whole surface of this domain (Toolbox of 3D patches in MATLAB). Then the total nuclear surface area was calculated by summing up the area of all triangles. These methods were validated by correctly calculating values for software-generated *z*-stack images of a 3D object with known volume and surface area. These methods were also validated by comparing the volume results to those obtained from Nikon NIS elements software. Supplementary material Movie 1 shows an example of a nucleus reconstructed from the experimental data.

Validation of volume measurements using spherical beads

We used *z*-slice confocal microscopy to obtain cell and nuclear volume measurements. To validate this approach, we also used the same microscope to measure volumes of spherical fluorescent beads. A volume standard with an irregular shape of similar size was not readily available to us. For 2-μm diameter beads (theoretical volume of 4.19 μm^3), our method yielded a mean volume of 4.69 μm^3, with a standard error of 1.19 μm^3 for n=51

(supplementary material Fig. S4). For 6-μm diameter beads (theoretical volume 113.04 μm^3), our method yielded a mean volume of 122.2 μm^3, with a standard error of 4.715 μm^3 for n=31. For 15-μm diameter beads (theoretical volume 1766.25 μm^3), our method yielded a mean volume of 1761 μm^3, with a standard error of 20.78 μm^3 for n=31.

Finite element simulations

We performed finite element simulations using the commercial software, ABAQUS (Version 6.10-1). At the adherent state, we used eight-node axi-symmetric hybrid reduced integration elements (CAX8RH) to mesh the nuclear envelope. The incompressible neo-Hookean constitutive model is adopted to characterize the non-linear response of the nucleus. For the critical buckling analysis, the same elements are used to mesh the nuclear envelope. The system contains about 10,000 elements. The BUCKLE function in ABAQUS is employed to perform the linear perturbation analysis and determine the critical characteristics of the first bifurcation. For the 3D shape evolution after the first bifurcation, eight-node 3D hybrid reduced integration elements (C3D8RH) are used to mesh the nuclear envelope. The system contains about 100,000 elements in total. A linear perturbation analysis is first performed. The obtained node displacements are multiplied by a small coefficient and introduced as pre-existing imperfections in the postbuckling analysis of the system. To avoid self-penetration, we introduced self-contact properties on both inner and outer surfaces of the envelope: the contact is frictionless in the tangential direction and is hard in the normal direction. We allow any possible separation after contact. The convergence of all simulations is carefully examined to ensure that the results are mesh independent.

Modeling nuclear volume and shape in the adherent state

The shape of the nucleus in adherent cells resembles a flat pancake. In this state, perinuclear actin stress fibers apply a compressive force F on the top of nucleus. Microtubules that fill the cytoplasmic space around the nucleus also exert forces. Given that the microtubules are dense and randomly distributed, we model this force as a pressure (P_{m0} in the adhered state) on the nucleus. The nucleus is also 'inflated' by the osmotic pressure difference ($\Delta\Pi_{n0}$ in the adhered state) across its envelope. Therefore, the total pressure difference across the nuclear envelope becomes $\Delta\Pi_{n0}-P_{m0}$. Given that the thickness-to-radius ratio for the nucleus is small ($\sim10^{-3}$–10^{-2}), and in the adherent state the nucleus deforms mostly by stretching, bending of the nuclear envelope can be ignored. We simplify the actin cap force as a compressive forces on the top of the nucleus, as shown in supplementary material Fig. S1. In the adherent state, the nuclear volume is static and the osmotic pressure difference is equal to the hydrostatic pressure difference (Eqn 1). Therefore, the mechanical force balance in the nuclear envelope can be stated as (Jiang and Sun, 2013):

$$(\Delta\Pi_{n0}-P_{m0})\pi r^2-2\pi rH\sigma\sin\theta-F=0, \tag{3}$$

where σ is the stress in the nuclear envelope and H is the thickness of nuclear envelope. Here, for simplification, we consider the small deformation case and changes in the envelope thickness, H, has been neglected. θ is the tangent angle of the nuclear envelope with respect to the vertical axis, as shown in supplementary material Fig. S1. Note that in this state, the nuclear volume is static and completely determined by the pressures and stresses in Eqn 3. In addition, in the adhered state, the nuclear volume is constant, and the osmotic pressure difference is equal to the hydrostatic pressure difference. Therefore $\Delta\Pi_{n0}$ appears in Eqn 3.

At the top of the nucleus, the contact angle θ between the nucleus and the actin cap is zero, therefore Eqn 3 yields:

$$F=(\Delta\Pi_{n0}-P_{m0})\pi r_a^2, \tag{4}$$

where r_a is the radius of the contacting region between the actin fibers and the nucleus. In the real situation, the contacting region is not a perfect circle. In our experiments and the theoretical model, r_a is estimated from the area of the contacting region. The average force per unit area applied by the actin stress fibers can be denoted as $P_F=F/(\pi r_a^2)$. From Eqn 3 we obtain:

$$r(\theta)=r_a\left(\beta\sin\theta+\sqrt{1+\beta^2\sin^2\theta}\right), \tag{5}$$

where:

$$\beta=\frac{\sigma H}{(\Delta\Pi_{n0}-P_{m0})r_a}. \tag{6}$$

From Eqn 5, the volume of the nucleus (V_n) can be calculated as:

$$V_n=\frac{2}{3}\pi r_a^3[(1+8\beta^2)E_2(\beta)-(1+4\beta^2)E_1(\beta)+\beta(3+8\beta^2)], \tag{7}$$

where E_1 and E_2 are, respectively, the complete elliptic integral of the first and second kind (Jeffrey and Zwillinger, 2007).

Given that V_{n0} and r_a can be measured from experiments, we can calculate β from Eqn 7. For example, in the adhered cell, the nuclear volume is ∼805 μm^3 and r_a is roughly 6.89 μm (Table 1), therefore β is 0.23.

Given that the nuclear envelope and the lamin network are elastic, the following neo-Hookean strain energy function, which is a non-linear, incompressible constitutive law, is used to describe the elastic response of nuclear envelope (Ogden, 1997):

$$W=\frac{\mu}{2}(\lambda_1^2+\lambda_2^2+\lambda_3^2-3), \tag{8}$$

where μ denotes the shear modulus and λ_i (i=1, 2, 3) are the principle stretch ratios of the nuclear envelope. Here, the nuclear envelope stretch is given by $\lambda=\sqrt{S_n/S_0}$, where S_n and S_0 are the surface areas of the nucleus in the current and the stress-free (reference) state, respectively. In the stress-free state, the nucleus prefers a spherical shape and the surface area is $S_0=4\pi A^2$, where A is the nuclear radius in the reference state. From the strain energy function in Eqn 8, the membrane stress is estimated as (Ogden, 1997):

$$\sigma=\mu\left(\frac{S_n}{S_0}-\frac{S_0^2}{S_n^2}\right), \tag{9}$$

Substituting Eqn 9 into Eqn 6 and using β derived from Eqn 7, we can obtain the total pressure difference across the nuclear envelope.

When the cell is treated with nocodazole, microtubules are removed but the actin cap remains on the top of the nucleus. In this case, the total pressure difference only contains contributions from the osmotic pressure and P_{m0}=0. It was found that during this process, the volume of the nucleus increased ∼5%, indicating that the microtubules apply a positive (compressive) pressure on the nucleus. The thickness of the nuclear envelope is H≈0.12 μm. The radius of the nucleus in the stress-free state is approximately A=5.75 μm. The experimental data before and after adding nocodazole are shown in supplementary material Table S1. Substituting the nuclear volume V_n and the contacting radius r_a given in supplementary material Table S1 into Eqn 7, we can compute β in absence of microtubules. Then, using the surface area S_n, we can calculate the (normalized) stress σ/μ from Eqn 9. Substituting this stress into Eqn 6, the osmotic pressure difference and the pressure applied by the microtubules can be estimated in terms of the data before and after treatment with nocodazole. Based on the data, we estimate that the pressure applied by the microtubules is $P_{m0}/\mu\approx2.33\times10^{-3}$ and the osmotic pressure difference is $\Delta\Pi_{n0}/\mu\approx8.39\times10^{-2}$. Therefore, in the adherent state, the total pressure difference is $P_0/\mu\approx8.16\times10^{-2}$, where $P_0=\Delta\Pi_{n0}-P_{m0}$. Our finite element simulations showed that this pressure difference (P_0) is necessary for maintaining the pancake-like shape of the nucleus, otherwise, the nucleus might invaginate laterally, as shown in Fig. 4B,C. With the total pressure difference, the average pressure applied by the actin fibers on top of the nucleus can be estimated from Eqn 4: $P_F/\mu\approx8.16\times10^{-2}$. If we take $\mu\sim10^4$ Pa, the force applied by the actin fibers is F≈122 nN. The microtubule compressive pressure, P_{m0}, is on the order of 20 Pa.

Modeling nuclear volume during cell detachment and suspension

Given that the nuclear volume is likely determined by the water content, the flow of water should determine the overall nuclear volume. The flux of water

Journal of Cell Science (2015) 128, 3375-3385 doi:10.1242/jcs.166330

across the nuclear envelope is primarily determined by the osmotic pressure difference ($\Delta\Pi_n$) and the hydrostatic pressure difference (ΔP_h) across the nuclear envelope, as expressed in Eqn 1. At mechanical equilibrium, the hydrostatic pressure difference must balance the mechanical stress in the nuclear envelope. The mechanical stress in the envelope, in turn, is a combination of the pressure applied by microtubules surrounding the nucleus (P_m, after actin remodeling) and the mechanical resistance of the nuclear envelope (P_r), that is, $\Delta P_h=P_m+P_r$.

During cell detachment and after actin remodeling, the cell volume reduced to nearly one half of its initial adhered state volume. We expressed the shrinkage in cell volume by $k=V_c/V_{c0}$, where V_{c0} and V_c are the cell volume before and after the cell is treated by trypsin, respectively. k is a function of time t, which can be fitted from the cell volume data, as shown in supplementary material Fig. S2.

The osmotic pressure is estimated by:

$$\Pi = \frac{NRT}{V}, \tag{10}$$

where N is the total number of solute, R is the gas constant, T is absolute temperature, and V is the volume of an enclosed vesicle. Note that for a crowded cellular cytoplasm, this expression for the osmotic pressure is only an estimate. The non-ideal aspect of osmotic pressure can be included using an activity coefficient. Nevertheless, the osmotic pressure must scale as V^{-1}. If we assume there is no substantial solute transport across the cell membrane during the detachment process, the osmotic pressure in the cytoplasm (Π_c) satisfies:

$$\frac{\Pi_c}{\Pi_{c0}} = \frac{V_{c0}}{V_c} = \frac{1}{k}, \tag{11}$$

where Π_{c0} is the cytoplasmic osmotic pressure outside the nucleus in the state before treated with trypsin. Similarly, if there is no solute transporting across the nuclear envelope, the osmotic pressure inside the nucleus (Π_n) is determined by:

$$\frac{\Pi_n}{\Pi_{n0}} = \frac{V_{n0}}{V_n}, \tag{12}$$

where V_n denotes the volume of the nucleus and the subscript 0 denotes the quantities in the attached state before treated with trypsin. Set $\Pi_{c0}=\zeta\Pi_{n0}$ with $0<\zeta<1$, then the osmotic pressure difference ($\Delta\Pi_n=\Pi_n-\Pi_c$) across the nuclear envelope can be expressed by:

$$\Delta\Pi_n = \left(\frac{V_{n0}}{V_n} - \frac{\zeta}{k}\right)\Pi_{n0}. \tag{13}$$

During cell detachment, microtubules gradually surround the whole nucleus and might also apply a time-dependent pressure on the nucleus. To model this, we approximately expressed the pressure applied by the microtubules as:

$$P_m = P_{m0} + P_{mi}(1 - e^{-gt}), \tag{14}$$

where g is a rate constant and P_{mi} is the total increment of pressure applied by the microtubules when the cell completely detached from the substrate. P_{m0} has been determined in the attached state (see above section). Our experiments showed that the cell became suspended after about 20 min. Hence, we fix g at 0.07 min^{-1}.

The mechanical resistance of the nuclear envelope is estimated by:

$$P_r = \frac{2\sigma H}{r}, \tag{15}$$

where r is the effective radius of the nucleus, which can be estimated from the volume of the nucleus. The membrane stress σ in the nuclear envelope, which correlates to the experimental measurement on the surface area change in the nuclear envelope (see the inset in Fig. 2C), is obtained from Eqn 9.

Substituting Eqns 13–15 into Eqn 1 leads to:

$$\frac{dV_n}{dt} = \alpha\left[\left(\frac{V_{n0}}{V_n} - \frac{\zeta}{k}\right)\Pi_{n0} - P_m - P_r\right]. \tag{16}$$

Eqn 16 can be rewritten as:

$$\frac{d\tilde{V}_n}{dt} = -\bar{\alpha}\left[\gamma\left(\frac{1}{1-\tilde{V}_n} - \frac{\zeta}{k}\right) - \bar{P}_m - \bar{P}_r\right], \tag{17}$$

where $\bar{\alpha} = \alpha\mu/V_{n0}$, $\tilde{V}_n = (V_{n0}-V_n)/V_{n0}$, $\gamma=\Pi_{n0}/\mu$, $\bar{P}_m = P_m/\mu$, and $\bar{P}_r$. $\bar{P}_r$ is calculated through Eqn 15. k has been fitted from measured change in cell volume (supplementary material Fig. S2). The osmotic pressure outside the cell is on the order $\sim 10^5$ Pa (Tinevez et al., 2009). Although there are no previous experiment data on the osmotic pressure inside the nucleus, the osmotic pressure inside the nucleus might be within the same order as the environmental osmotic pressure outside the cell. The elastic modulus of nuclear envelope varies substantially, depending on the cell type, the cell cycle phase, the measurement method and so on. For example, by using micropipette aspiration, the elastic modulus of the whole nucleus inside pig chondrocyte is ~1 kPa (Guilak et al., 2000). However, we believe that when the nucleus is compressed to a large extent, material such as chromatin inside the nucleus might play an important role in defining the effective elastic modulus of the nucleus. Previous experiments have shown that the elastic modulus of mitotic chromosomes in newt lung cells is in the range of 1×10^5–5×10^5 Pa (Houchmandzadeh et al., 1997). Based on these factors, the ratio between the osmotic pressure (Π_{n0}) inside the nucleus and the elastic modulus (μ) of the envelope might be in the range $\gamma\approx1$–100. From $\Delta\Pi_{n0}=(1-\zeta)\Pi_{n0}$ and $\gamma=\Pi_{n0}/\mu$, we obtained $\zeta=1-\Delta\Pi_{n0}/(\gamma\mu)$. Given that we know $\Delta\Pi_{n0}/\mu\approx8.39\times10^{-2}$ from the attached state (see above section), we express ζ as $\zeta=1-8.39\times10^{-2}/\gamma$. There remain three unknowns, i.e. $\bar{\alpha}$, γ and $\bar{P}_{mi}$ ($=P_{mi}/\mu$), that are needed to solve Eqn 17. It can be observed from Eqn 17 that $\bar{\alpha}$ is a constant describing how fast the nucleus arrives at the steady state but does not influence the value of the steady volume. Hence, $\bar{\alpha}$ can be fitted in terms of the slope of $\bar{V}_n(t)$ before the nucleus arrives at the steady state. Based on our experiments, we find $\gamma\sim50$ and $\bar{P}_{mi}\approx0.16\times10^{-3}$ best explain our data. Therefore, when the nucleus reached a stable volume in the suspended state, the total pressure applied by the microtubules is $\bar{P}_m\approx2.49\times10^{-3}$. The relevant physical parameters shaping the nucleus are summarized in supplementary material Table S1.

When we treated the cells with both trypsin and nocodazole, the cell detached from the substrate and, at the same time, microtubules surrounding the nucleus were eliminated. In other words, the pressure applied by the microtubules (P_m) was removed. Similarly, the volume of the nucleus decreased (see Fig. 2D) and the nuclear envelope wrinkled. However, the volumetric shrinkage was less than that in cells treated with trypsin only. Again, this confirms that microtubules apply a compressive pressure on the nucleus. To estimate the average stable radius of the nucleus in this case, we approximated the nucleus as a sphere. Then, the nuclear volume and surface area can be calculated through $V_n=4\pi r^3/3$ and $S_n=4\pi r^2$. Using the same parameters (k, γ and $\Delta\Pi_{n0}/\mu$) obtained from the previous analysis, we estimate that the average radius of the nucleus after treated with both trypsin and nocodazole is $r\approx4.63$ μm, agreeing with estimates from our experimental data ($r\approx4.87$μm). These measurements suggest that the microtubule network also exerts compressive forces on the nucleus.

In live cells, many proteins, RNAs and ions are trafficked across the nuclear envelope. A sum of these fluxes is not available, but the net flux is likely to be small when compared with the total molecular content of the nucleus. Therefore, in our analysis, we have assumed that the nuclear osmolyte content is constant with good results. With higher resolution measurements, it is conceivable to develop more accurate models. Nevertheless, we believe that the osmotic pressure and cytoskeletal motor force are principal elements defining the shape and volume of the eukaryotic nucleus.

Competing interests

The authors declare no competing or financial interests.

Author contributions

D.-H.K., B.L., D.W. and S.X.S. designed the research, D.-H.-K., B.L., F.S., J.M.P. performed the experiments and data analysis. B.L. performed the model computations. B.L., D.-H.K., D.W. and S.X.S. wrote the paper.

Funding
This research is supported by the National Science Foundation (NSF) [grant number PHY-1205795]; and the National Institutes of Health [grant number 1U54CA143868]. Deposited in PMC for release after 12 months.

Supplementary material
Supplementary material available online at
http://jcs.biologists.org/lookup/suppl/doi:10.1242/jcs.166330/-/DC1

References

Abu-Arish, A., Kalab, P., Ng-Kamstra, J., Weis, K. and Fradin, C. (2009). Spatial distribution and mobility of the ran gtpase in live interphase cells. *Biophys. J.* **97**, 2164-2178.
Aebi, U., Cohn, J., Buhle, L. and Gerace, L. (1986). The nuclear lamina is a meshwork of intermediate-type filaments. *Nature* **323**, 560-564.
Beaudouin, J., Gerlich, D., Daigle, N., Eils, R. and Ellenberg, J. (2002). Nuclear envelope breakdown proceeds by microtubule-induced tearing of the lamina. *Cell* **108**, 83-96.
Ben Amar, M. and Goriely, A. (2005). Growth and instability in elastic tissues. *J. Mech. Phys. Solids* **53**, 2284-2319.
Bissell, M. J., Weaver, V. M., Lelièvre, S. A., Wang, F., Petersen, O. W. and Schmeichel, K. L. (1999). Tissue structure, nuclear organization, and gene expression in normal and malignant breast. *Cancer Res.* **59**, 1757-1764.
Buxboim, A., Ivanovska, I. L. and Discher, D. E. (2010). Matrix elasticity, cytoskeletal forces and physics of the nucleus: how deeply do cells 'feel' outside and in? *J. Cell. Sci.* **123**, 297-308.
Buxboim, A., Swift, J., Irianto, J., Spinler, K. R., Dingal, P. C. D. P., Athirasala, A., Kao, Y.-R. C., Cho, S., Harada, T., Shin, J.-W. et al. (2014). Matrix elasticity regulates lamin-a.c. phosphorylation and turnover. *Curr. Biol.* **24**, 1909-1917.
Chow, K.-H., Factor, R. E. and Ullman, K. S. (2012). The nuclear envelope environment and its cancer connections. *Nat. Rev. Cancer* **12**, 196-209.
Dahl, K. N., Kahn, S. M., Wilson, K. L. and Discher, D. E. (2004). The nuclear envelope lamina network has elasticity and a compressibility limit suggestive of a molecular shock absorber. *J. Cell Sci.* **117**, 4779-4786.
Dahl, K. N., Ribeiro, A. J. S. and Lammerding, J. (2008). Nuclear shape, mechanics, and mechanotransduction. *Circ. Res.* **102**, 1307-1318.
Datta, S. S., Kim, S.-H., Paulose, J., Abbaspourrad, A., Nelson, D. R. and Weitz, D. A. (2012). Delayed buckling and guided folding of inhomogeneous capsules. *Phys. Rev. Lett.* **109**, 134302.
Dauer, W. T. and Worman, H. J. (2009). The nuclear envelope as a signaling node in development and disease. *Dev. Cell* **17**, 626-638.
Funkhouser, C. M., Sknepnek, R., Shimi, T., Goldman, A. E., Goldman, R. D. and Olvera de la Cruz, M. (2013). Mechanical model of blebbing in nuclear lamin meshworks. *Proc. Natl. Acad. Sci. USA* **110**, 3248-3253.
Georges, P. C., Miller, W. J., Meaney, D. F., Sawyer, E. S. and Janmey, P. A. (2006). Matrices with compliance comparable to that of brain tissue select neuronal over glial growth in mixed cortical cultures. *Biophys. J.* **90**, 3012-3018.
Gerlitz, G., Reiner, O. and Bustin, M. (2013). Microtubule dynamics alter the interphase nucleus. *Cell. Mol. Life Sci.* **70**, 1255-1268.
Guilak, F., Tedrow, J. R. and Burgkart, R. (2000). Viscoelastic properties of the cell nucleus. *Biochem. Biophys. Res. Commun.* **269**, 781-786.
Gundersen, G. G. and Worman, H. J. (2013). Nuclear positioning. *Cell* **152**, 1376-1389.
Hampoelz, B., Azou-Gros, Y., Fabre, R., Markova, O., Puech, P.-H. and Lecuit, T. (2011). Microtubule-induced nuclear envelope fluctuations control chromatin dynamics in drosophila embryos. *Development* **138**, 3377-3386.
Houchmandzadeh, B., Marko, J. K., Chatenay, D. and Libchaber, A. (1997). Elasticity and structure of eukaryote chromosomes studied by micromanipulation and micropipette aspiration. *J. Cell Biol.* **139**, 1-12.
Hutchinson, J. W. (1967). Imperfection sensitivity of externally pressurized spherical shells. *ASME J. Appl. Mech.* **34**, 49-55.
Irianto, J., Swift, J., Martins, R. P., McPhail, G. D., Knight, M. M., Discher, D. E. and Lee, D. A. (2013). Osmotic challenge drives rapid and reversible chromatin condensation in chondrocytes. *Biophys. J.* **104**, 759-769.
Jeffrey, A. and Zwillinger, A. (2007). *Gradshteyn and Ryzhik's Table of Integrals, Series, and Products*. New York: Academic Press.
Jiang, H. and Sun, S. X. (2013). Cellular pressure and volume regulation and implications for cell mechanics. *Biophys. J.* **105**, 609-619.
Khatau, S. B., Hale, C. M., Stewart-Hutchinson, P. J., Patel, M. S., Stewart, C. L., Searson, P. C., Hodzic, D. and Wirtz, D. (2009). A perinuclear actin cap regulates nuclear shape. *Proc. Natl. Acad. Sci. USA* **106**, 19017-19022.
Kim, D.-H. and Wirtz, D. (2015). Cytoskeletal tension induces the polarized architecture of the nucleus. *Biomaterials* **48**, 161-172.
Kim, D.-H., Chambliss, A. B. and Wirtz, D. (2013). The multi-faceted role of the actin cap in cellular mechanosensation and mechanotransduction. *Soft Matter* **9**, 5516-5523.
Kim, D.-H., Cho, S. and Wirtz, D. (2014). Tight coupling between nucleus and cell migration through the perinuclear actin cap. *J. Cell Sci.* **127**, 2528-2541.
Lammerding, J., Hsiao, J., Schulze, P. C., Kozlov, S., Stewart, C. L. and Lee, R. T. (2005). Abnormal nuclear shape and impaired mechanotransduction in emerin-deficient cells. *J. Cell Biol.* **170**, 781-791.
Laporte, D., Courtout, F., Salin, B., Ceschin, J. and Sagot, I. (2013). An array of nuclear microtubules reorganizes the budding yeast nucleus during quiescence. *J. Cell Biol.* **203**, 585-594.
Lidmar, J., Mirny, L. and Nelson, D. R. (2003). Virus shapes and buckling transitions in spherical shells. *Phys. Rev. E* **68**, 051910.
Macara, I. G. (2001). Transport into and out of the nucleus. *Microbiol. Mol. Biol. Rev.* **65**, 570-594.
Maeshima, K., Iino, H., Hihara, S., Funakoshi, T., Watanabe, A., Nishimura, M., Nakatomi, R., Yahata, K., Imamoto, F., Hashikawa, T. et al. (2010). Nuclear pore formation but not nuclear growth is governed by cyclin-dependent kinases (cdks) during interphase. *Nat. Strut. Mol. Biol.* **17**, 1065-1071.
Munevar, S., Wang, Y.-L. and Dembo, M. (2001). Traction force microscopy of migrating normal and h-ras transformed 3t3 fibroblasts. *Biophys. J.* **80**, 1744-1757.
Ogden, R. W. (1997). *Non-linear Elastic Deformations*. New York: Dover Publications.
Panorchan, P., Schafer, B. W., Wirtz, D. and Tseng, Y. (2004). Nuclear envelope breakdown requires overcoming the mechanical integrity of the nuclear lamina. *J. Biol. Chem.* **279**, 43462-43467.
Quemeneur, F., Quilliet, C., Faivre, M., Viallat, A. and Pépin-Donat, B. (2012). Gel phase vesicles buckle into specific shapes. *Phys. Rev. Lett.* **108**, 108303.
Roca-Cusachs, P., Alcaraz, J., Sunyer, R., Samitier, J., Farre, R. and Navajas, D. (2008). Micropatterning of single endothelial cell shape reveals a tight coupling between nuclear volume in g1 and proliferation. *Biophys. J.* **94**, 4984-4995.
Sabass, B., Gardel, M. L., Waterman, C. M. and Schwarz, U. S. (2008). High resolution traction force microscopy based on experimental and computational advances. *Biophys. J.* **94**, 207-220.
Salbreux, G., Joanny, J. F., Prost, J. and Pullarkat, P. (2007). Shape oscillations of non-adhering fibroblast cells. *Phys. Biol.* **4**, 268-284.
Shimi, T., Butin-Israeli, V., Adam, S. A. and Goldman, R. D. (2010). Nuclear lamins in cell regulation and disease. *Cold Spring Harb. Symp. Quant. Biol.* **75**, 525-531.
Simon, D. N. and Wilson, K. L. (2011). The nucleoskeleton as a genome-associated dynamic 'network of networks'. *Nat. Rev. Mol. Cell Biol.* **12**, 695-708.
Swift, J., Ivanovska, I. L., Buxboim, A., Harada, T., Dingal, P. C. D. P., Pinter, J., Pajerowski, J. D., Spinler, K. R., Shin, J.-W., Tewari, M. et al. (2013). Nuclear lamin-a scales with tissue stiffness and enhances matrix-directed differentiation. *Science* **341**, 1240104.
Tamura, K., Iwabuchi, K., Fukao, Y., Kondo, M., Okamoto, K., Ueda, H., Nishimua, M. and Hara-Nishimura, I. (2013). Myosin xi-i links the nuclear membrane to the cytoskeleton to control nuclear movement and shape in arabidopsis. *Curr. Biol.* **23**, 1776-1781.
Tinevez, J.-Y., Schulze, U., Salbreux, G., Roensch, J., Joanny, J.-F. and Paluch, E. (2009). Role of cortical tension in bleb growth. *Proc. Natl. Acad. Sci. USA* **106**, 18581-18586.
Vaziri, A., Lee, H. and Kaazempur Mofrad, M. R. (2006). Deformation of the cell nucleus under indentation: mechanics and mechanisms. *J. Mater. Res.* **21**, 2126-2135.
Versaevel, M., Grevesse, T. and Gabriele, S. (2012). Spatial coordination between cell and nuclear shape within micropatterned endothelial cells. *Nat. Commun.* **3**, 671.
Weiss, P. and Garber, B. (1952). Shape and movement of mesenchyme cells as functions of the physical structure of the medium: contributions to a quantitative morphology. *Proc. Natl. Acad. Sci. USA* **38**, 264-280.
Wirtz, D., Konstantopoulos, K. and Searson, P. C. (2011). The physics of cancer: the role of physical interactions and mechanical forces in metastasis. *Nat. Rev. Cancer* **11**, 512-522.
Zhao, T., Graham, O. S., Raposo, A. and St Johnston, D. (2012). Growing microtubules push the oocyte nucleus to polarize the drosophila dorsal-ventral axis. *Science* **336**, 999-1003.
Zink, D., Fischer, A. H. and Nickerson, J. A. (2004). Nuclear structure in cancer cells. *Nat. Rev. Cancer* **4**, 677-687.

Supplemental material

Supplemental Table S1

Table S1: Summary of parameters estimated from measurements and theory

Parameter	Description	Value	Note
$\Delta\Pi_{n0}$	Osmotic pressure difference across the nuclear envelope in the adherent state (Pa)	839[a]	Solved
F	Force applied by actin fibers atop the nucleus in the adherent state (nN)	122[a]	Solved
P_{m0}	Pressure applied by microtubules in the adherent state (Pa)	23.3[a]	Solved
P_{mi}	Increased pressure applied by microtubules in the suspended state (Pa)	1.6[a]	Fitted
$\gamma = \Pi_{n0}/\mu$	Ratio between the osmotic pressure inside the nucleus and the shear modulus of the nucleus	50	Fitted
$\bar{\alpha}$	Rate constant of water transport (min^{-1})	3×10^{-3}	Fitted

[a]The shear modulus of the nuclear envelope has been taken as $\mu \sim 10^4$Pa

Supplemental Figures

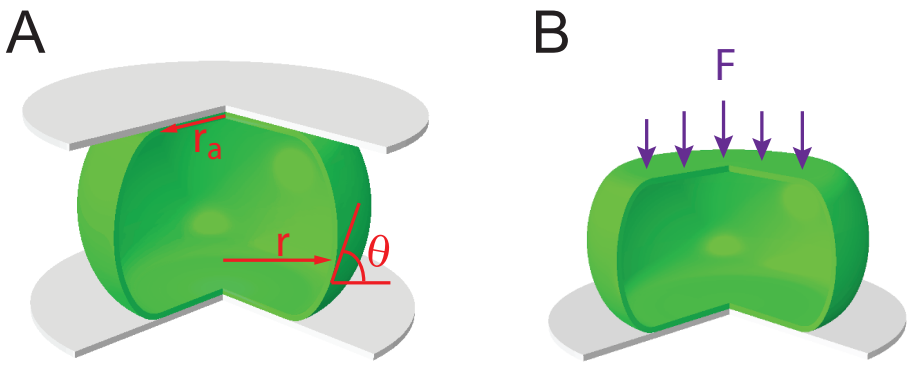

Figure S1: Schematic of the cell nucleus in the attached state. (A) We model the compression force from perinuclear actin stress fibers as a compressive plate. (B) The total force from actin stress fibers is F.

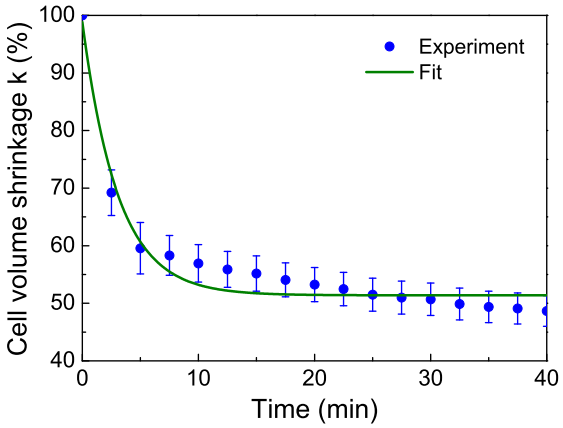

Figure S2: Shrinkage in MEF cell volume during detachment from the substrate as computed from $k(t) = V_c(t)/V_{c0}$ (standard errors are computed from 37 cells). The volume decreased by 50%. The green line is a numerical fit to the data, which is then used in Eq. 17 to compute the nuclear volume.

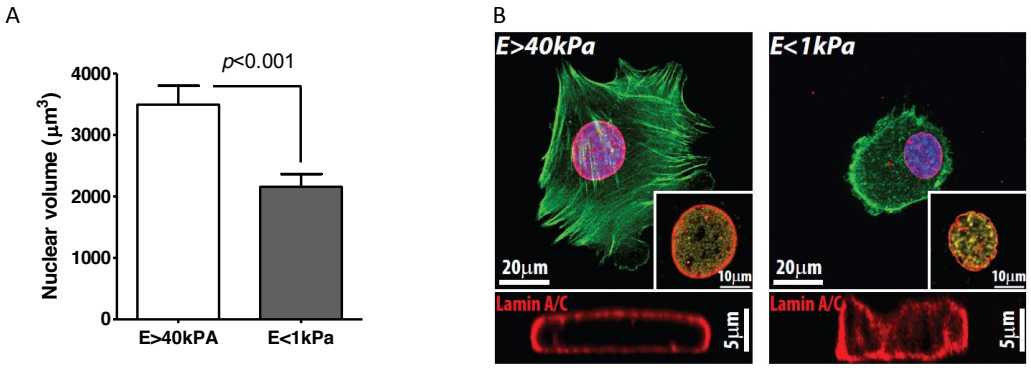

Figure S3: Nuclear volume change in MEF cells on substrates of different stiffness. (A) Average nuclear volume for cells on stiff ($E > 40$kPa) and soft ($E <1$kPa) polyacrylamide hydrogels. $N > 20$ cells were tested per condition (B) 3D reconstructed images of cell nuclei on stiff and soft substrates. Images are modified from Fig. 3J and K in Kim and Wirtz (2015).

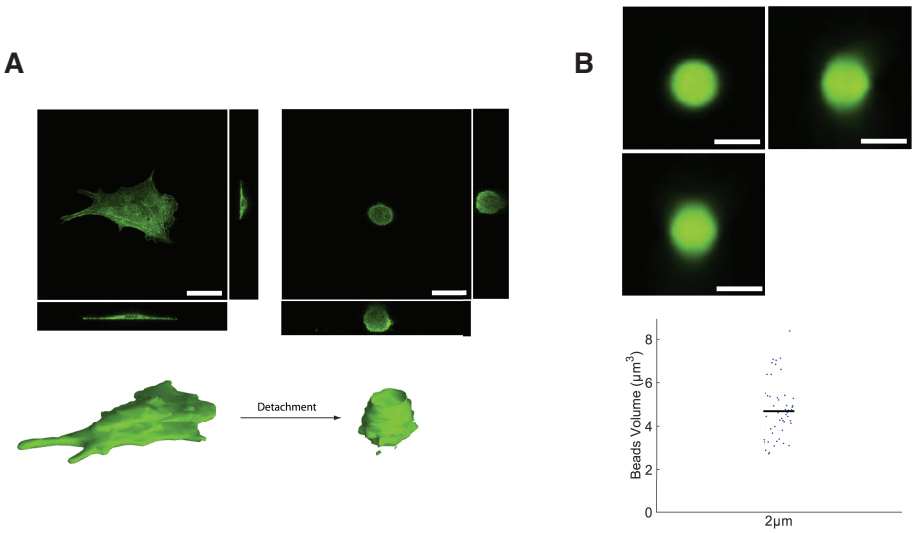

Figure S4: (A) 3D confocal images of MEF cells in attached and detached state. The reconstructed shapes are shown below. The scale bar is 30μm. (B) 3D confocal images of 2μm diameter beads. The scale bar is 2μm. The average computed volume is within 10% of the theoretical volume, but there are significant measurement errors for small beads.

Supplemental Movies

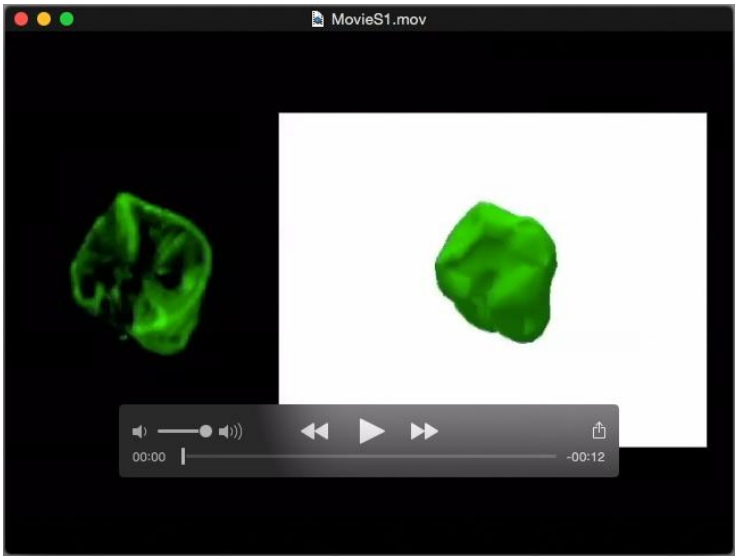

Movie 1 A movie comparing the 3D confocal images of the nucleus with the 3D reconstructed nucleus.